AUV Observations of the Diurnal Surface Layer in the North Atlantic Salinity Maximum

BENJAMIN A. HODGES AND DAVID M. FRATANTONI

Woods Hole Oceanographic Institution, Woods Hole, Massachusetts

(Manuscript received 19 June 2013, in final form 7 March 2014)

ABSTRACT

Autonomous underwater vehicle (AUV) surveys of temperature, salinity, and velocity in the upper 10 m of the ocean were carried out in low-wind conditions near the North Atlantic surface salinity maximum as part of the Salinity Processes in the Upper Ocean Regional Study (SPURS) project. Starting from a well-mixed state, the development, deepening, and decay of a warm salty diurnal surface layer was observed at <1-h resolution. The evaporation rate deduced from the freshwater anomaly of the layer corroborates measurements at a nearby flux mooring. Profiles within a few hundred meters of the stationary research vessel showed evidence of mixing, highlighting the effectiveness of AUVs for collecting uncontaminated time series of near-surface thermohaline structure. A two-dimensional horizontal subsurface survey within the diurnal warm layer revealed coherent warm and cool bands, which are interpreted as internal waves on the diurnal thermocline.

1. Introduction/motivation

Changes in sea surface temperature (SST) strongly impact air–sea fluxes and atmospheric convection (e.g., Jacobs 1942), making the dynamics of the ocean's diurnal warm layer an important component of the coupled ocean–atmosphere system. Under low-wind conditions with strong solar heating, the ocean surface occasionally warms by 3°C or more over the course of a day (e.g., Stramma et al. 1986; Webster et al. 1996); often the temperature increase is initially confined to the upper meter (Price et al. 1986; Soloviev and Lukas 1997), decaying exponentially with depth (Halpern and Reed 1976). The stabilizing effect of the thermal stratification then inhibits convection and vertical mixing, allowing evaporation to produce a measurable increase in surface salinity (Soloviev and Lukas 1997). The daytime warming and salinification characterizing this low-wind diurnal cycle, as well as the associated enhancement of horizontal thermohaline variability at the surface, have implications for the interpretation of satellite observations of sea surface temperature (e.g., Stuart-Menteth et al. 2003) and salinity.

Unambiguously resolving physical processes occurring within the diurnal warm layer often requires capturing small-scale three-dimensional variability or time evolution of vertical profiles. However, repeated observations of this thermohaline structure are difficult to make from a research vessel, as the vessel itself quickly erases the warm surface signature by inducing vertical mixing (Fig. 1). Even smaller platforms can cause significant disruption: Farrar et al. (2007) report a ~300-m-long cool wake downstream of a 3-m mooring buoy in airborne infrared measurements of SST under low winds; near-surface temperature sensors on such moorings typically indicate little stratification in the upper meter, even under low-wind, high-insolation conditions (see, e.g., Walsh et al. 1998, their Figs. 14 and 16).

To avoid contaminating the measurements, research vessel–based sampling of the low-wind diurnal warm layer must either be made while constantly moving into undisturbed water, precluding repeat observations, or with small instrument packages deployed at a distance from the vessel. Effective measurements have been made from free-rising profilers, but ensuring these are completely out of the research vessel's footprint is challenging—vessel contamination may be indistinguishable from wind mixing. For examples of observations of both types—bow probes mounted forward of a research vessel and profiles collected by a free-rising instrument package—refer to Soloviev and Lukas (1997).

Corresponding author address: Benjamin A. Hodges, 266 Woods Hole Rd., MS 30, Woods Hole, MA 02543.
E-mail: bhodges@whoi.edu

DOI: 10.1175/JPO-D-13-0140.1

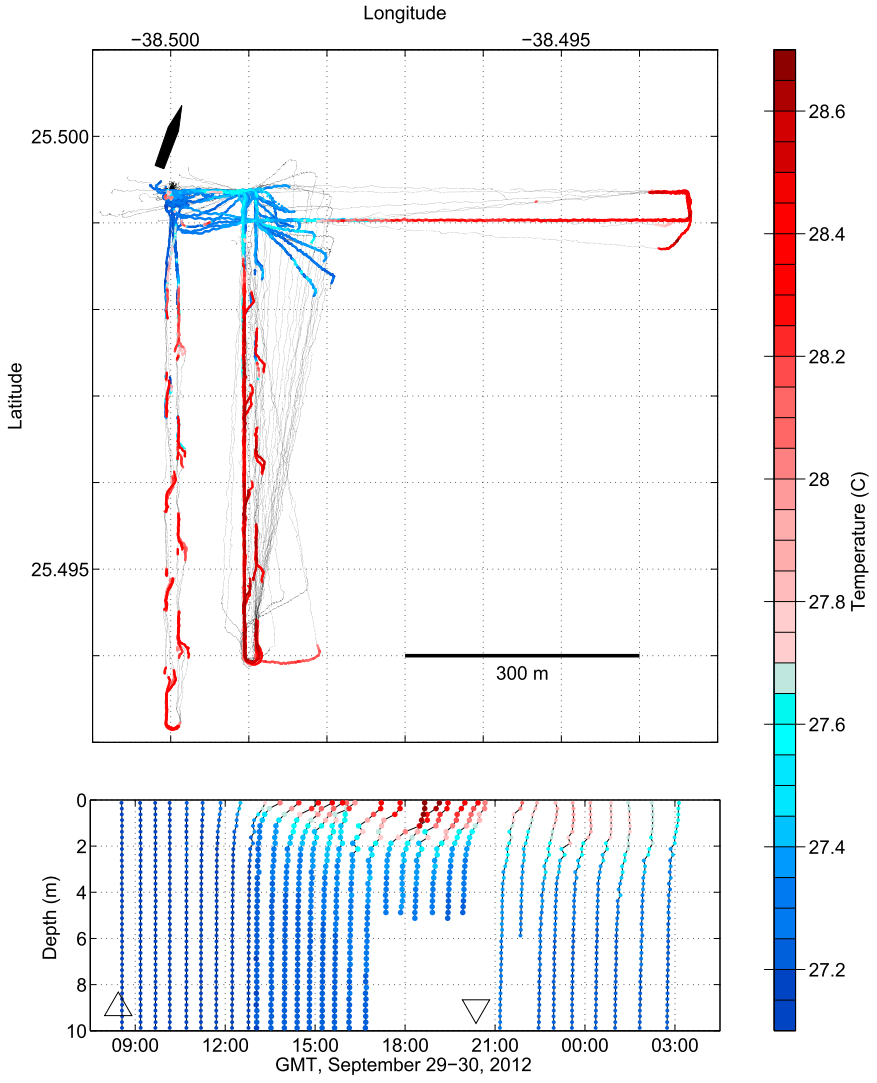

FIG. 1. Temperature observed during a sequence of AUV operations on a calm day. (top) Tracks from all 33 missions; temperatures of the upper 30 cm observed between 1300 and 2000 UTC (the period of max stratification) are indicated by color. Segments of the tracks from other time periods and deeper layers are drawn lightly. (bottom) The 25-cm bin-averaged temperature profile, excluding contaminated measurements near the ship, for each of the 33 missions. Each profile is plotted at the time it was measured, with larger colored markers indicating the period corresponding to temperatures plotted in the upper panel. The horizontal scaling of temperature is 1°C = 1 h. Sunrise and sunset are indicated by upward and downward triangles, respectively.

Here, we present observations made from Iver2/EcoMapper autonomous underwater vehicles (AUVs), which, due to their small size, accurate maneuverability, and relatively high speed, are able to repeatedly sample the diurnal warm layer without inducing significant mixing. These measurements are described in section 2. Section 3 presents an analysis of the low-wind diurnal cycle of temperature and salinity, spanning nearly a day at <1-h resolution. Internal waves observed in subsurface measurements within the diurnal warm layer are investigated in section 4. Conclusions are presented in section 5.

2. Methods

The results presented here are based primarily on temperature and salinity observations of the upper 10 m of the ocean, made under low-wind conditions from Iver2/EcoMapper AUVs on 29 and 30 September 2012 as part of the Salinity Processes in the Upper Ocean

Regional Study (SPURS) project. The fall 2012 SPURS cruise focused an intensive observational effort on the hydrography and microstructure of the upper layer of the ocean in the region of the North Atlantic salinity maximum, near 25°N, 38°W. A wide variety of mobile platforms were employed in conjunction with ship-based conductivity–temperature–depth (CTD) casts. In addition, three moorings were deployed, including the heavily instrumented "SPURS flux mooring," from which can be derived estimates of the fluxes of momentum, heat, and water across the ocean–atmosphere interface. These flux estimates provide a consistency check for some of the following AUV results (section 3, below).

The Iver2 is a small (~30 kg) propeller-driven AUV manufactured by OceanServer Technology, Inc. (Fall River, MA). YSI, Inc. (Yellow Springs, OH), supplements this base vehicle with a suite of their environmental sensors and sells it as the EcoMapper. At a maximum underwater speed of 1.8 m s^{-1}, the AUV has an endurance of approximately 5 h.

Consecutive observational missions a few hundred meters from the research vessel were run for longer periods without interruption by alternating two vehicles between active duty and on-deck battery recharging. The AUVs navigate by global positioning system (GPS) at the surface and by compass, tilt sensor, and a six-beam SonTek Doppler velocity log (DVL) when submerged. The DVL, with four down-looking beams operating at 1 MHz and an upward- and downward-looking pair at 500 kHz, measures both speed through the water and depth from the surface; an independent estimate of the vertical position of the vehicle is obtained by measuring pressure. The estimates of horizontal position underwater rely on dead reckoning and are adjusted in postprocessing to account for the inferred average current velocity while submerged, locating the measurements more accurately. This current estimate for an underwater leg is calculated from the length of time spent underwater and the distance between two concurrent position estimates when the vehicle resurfaces: 1) the dead-reckoned position, which is based on the final GPS fix before submerging to begin the leg, the vehicle's speed through the water, and heading and attitude information; and 2) the new GPS position.

The vehicles are equipped with both YSI and Neil Brown Ocean Sensors, Inc. (NBOS), CTD sensors; here we use measurements made by the NBOS CTD, which offers higher precision (0.001 psu). Prior to the cruise, these temperature and conductivity sensors were calibrated against pumped Sea-Bird Electronics sensors (SBE 3 and 4). EcoMappers log temperature, conductivity, pressure, and horizontal position data at a frequency of 1 Hz.

A number of operations were required to improve the accuracy of the raw NBOS salinity measurements. Standard methods were applied to eliminate glitches associated with bubbles and salinity spiking due to sensor geometry and response time. Shipboard measurements were used to correct for conductivity sensor drift. Following Morison et al. (1994), we also applied an iterative correction to the measured temperature, compensating for the thermal mass of the conductivity cell, before using it to compute salinity. Two parameters are involved in this procedure: β^{-1} is the cell thermal equilibration time constant, and α is the initial temperature error as a fraction of a hypothetical step-function temperature variation. The values $\beta = 0.15\,s^{-1}$ and $\alpha = 0.015$ were chosen to eliminate, by eye, the average temperature–salinity (T–S) curve bias between fully processed upward and downward profiles.

3. Diurnal warming cycle

Early on the morning of 29 September 2012, the 85-m Research Vessel (R/V) *Knorr* began holding station at 25°30′N, 38°30′W, using automated dynamic positioning. At 0820 UTC, just after dawn, EcoMapper missions commenced, continuing at quasi-regular intervals for the next 18.5 h. Each of the 33 missions lasted approximately 20 min and consisted of an outward leg to a distance of 600–700 m from the ship and a return leg with a nominal horizontal offset of 15 m (actual separation varied depending on currents—estimated tracks are plotted in Fig. 1 and shipboard ADCP measurements of upper-ocean currents are in Fig. 2). The outbound legs were run either at the surface, at a constant depth of 1 m, or undulating between depths of 0 and 5 m. All of the return legs were undulating either between 0 and 5 or 0 and 10 m. The majority of the missions, 28, ran to the south from the research vessel's position; the remaining 5 ran to the east. Winds were light and skies were clear; shipboard measurements from dual sensors 15.5 m above the water line indicate that wind speed remained under 2 m s^{-1} for nearly the entire sampling period (Fig. 2), and estimated net heat flux into the ocean at the SPURS flux mooring, 110 km to the south-southwest of the EcoMapper study site, reached a maximum of 675 W m^{-2} at midday.

In the morning, the surface layer was well mixed. In the calm sunny conditions, significant stratification developed in the upper meter by midday. This stratification strengthened and deepened during the afternoon, reaching total surface increases of 1.5°C in temperature and 0.02 psu in salinity. Toward sunset it began to decay, and by 0200 local time, the stratification had weakened considerably, particularly in temperature (Fig. 1, bottom).

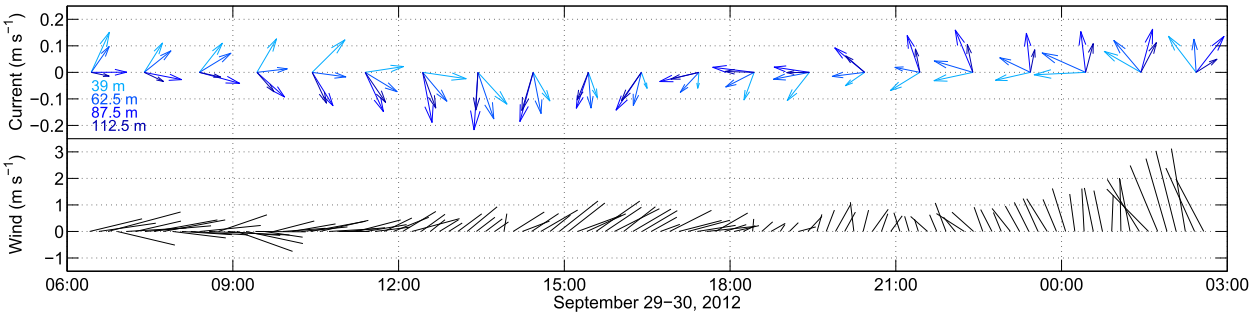

FIG. 2. (top) Hourly averages of four 25-m depth bins of current velocity measured by a 75-kHz shipboard ADCP while the ship was on station for AUV operations. The current vectors rotate clockwise with time at approximately the inertial frequency and also clockwise with increasing depth. (bottom) The 10-min averages of the wind velocity observed during the same period. Plotted vectors are averages of the output of two sensors on either side of the bow mast, 15.5 m above the water line. Throughout most of the experiment, wind speed was less than 2 m s^{-1}. An upward vector represents a northward velocity.

To capture the evolution of this diurnal stratification, it is important to sample undisturbed water, far enough from the ship to avoid the churning of its propellers and the mixing it causes as it bobs in the waves. The homogenizing influence of the ship is obvious as a cool surface signature out to a radius of over two ship lengths (Fig. 1, top). To avoid this contamination, composite profiles from each mission, both those plotted in Fig. 1 and those used in the analysis to follow, are formed by averaging observations into vertical bins after excluding any measurements made within 300 m of the ship. The slight temperature inversions apparent in many of the profiles are artifacts of this process: combining horizontally and temporally separated measurements into a single profile increases the vertical resolution at the expense of some noise due to the horizontal variability and vertical fluid motion. Although the wake of the ship undoubtedly extended farther than 300 m in the direction of the prevailing current, this threshold was sufficient to eliminate nearly all evidence of ship-induced mixing at the locations sampled.

Though the time series is of course not Lagrangian—changes from one profile to the next reflect spatial variability advected by prevailing currents as well as temporal evolution—we ignore the contribution of advection here. Upper-ocean current speeds were rather small (<15 cm s^{-1}; see Fig. 2), meaning that the horizontal displacement of a water parcel in the interval between one AUV mission and the next was smaller than the length scale spanned by the mission itself.

The diurnal signal in salinity is weaker than that in temperature, both in terms of its effect on density and relative to the sensitivity of the sensor, but the influence of evaporation is clear (Fig. 3). Early in the day (green profiles in Fig. 3; 0909 UTC, ~45 min after sunrise), the sampled water column was nearly homogenous. At midday (cyan profiles in Fig. 3; 1538 UTC, ~1 h and 15 min after solar zenith), the salty surface layer was confined to the upper meter, with a more surface-compressed profile than that of temperature; presumably, the stability provided by the temperature stratification suppressed the convection that would otherwise occur, initially trapping the evaporation signature quite near the surface. By early evening (blue profiles in Fig. 3; 2139 UTC, ~1 h and 15 min after sunset), the high-salinity signature had extended to a depth of 4 m, matching the vertical structure of the concurrent temperature profile as both properties mixed downward. Later in the evening (magenta profiles in Fig. 3; 0150 UTC, ~30 min before solar nadir), the vertical gradients just below the surface decreased as the ocean lost heat to the atmosphere, and the upper meters began to homogenize, likely under the influence of both convection and wind-driven mixing, though the experiment was terminated before this process was complete.

Once a stable warm layer has formed, vertically integrating the positive salinity anomaly over the layer provides an estimate of the total evaporation following the development of the stratification (Fig. 3c). The changes in salinity within the bulk mixed layer observed during the day were presumably the result of the advection of horizontal variability, so salinity anomalies are calculated relative to the concurrently measured 10-m value. Preliminary analysis of concurrent measurements from the SPURS flux mooring provides an independent estimate of evaporation (T. Farrar 2013, personal communication) at a relatively nearby (on meteorological scales) location. The freshwater anomaly calculated by time integration of these observations, starting at 1000 UTC, when thermal stratification first appeared, agrees well with the AUV-based estimate (Fig. 3d), with both suggesting an average evaporation rate of ~2.8 mm day^{-1} over the lifetime of the layer. Throughout the day, the excess heat content of the surface

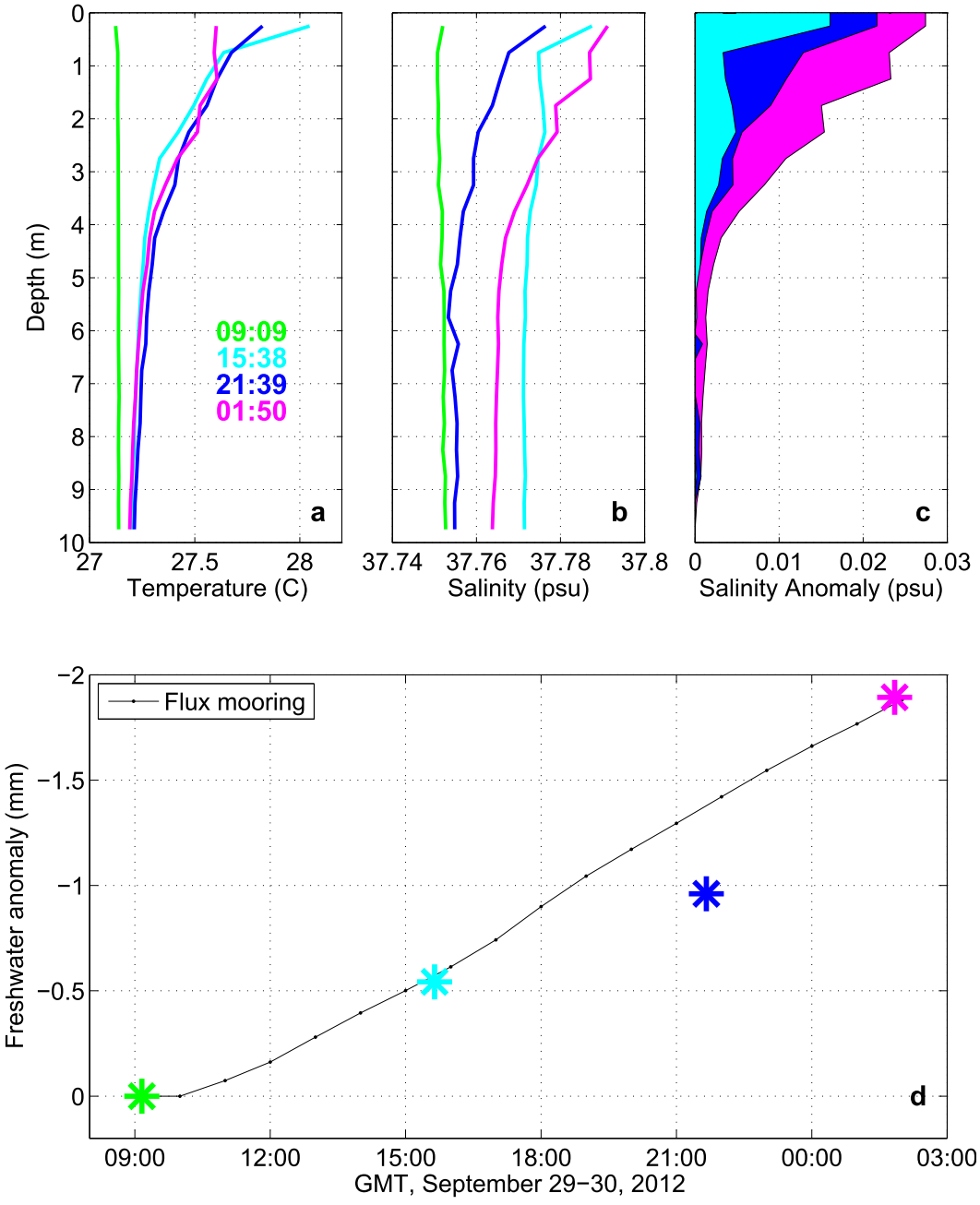

FIG. 3. (a) Half-meter bin-averaged temperature profiles formed from four sets of three consecutive AUV missions, excluding observations closer than 300 m to the research vessel (individual temperature profiles shown in Fig. 1). The mean time (UTC) of the measurements forming each profile is displayed in the corresponding color. (b) Average salinity profiles, plotted as in (a). (c) Salinity anomaly, relative to the 10-m value, of the profiles in (b). (d) Freshwater anomalies implied by the vertically integrated salinity anomalies from (c). Time-integrated evaporation calculated from air–sea flux measurements made at a mooring 110 km away is shown in black as a comparison.

layer implied by its temperature increase relative to a depth of 10 m (not shown) is about half the cumulative estimated net heat flux into the ocean, integrated from 1000 UTC onward. Not all the heat is trapped in the stable warm layer, as some radiation is absorbed below it.

Under calm sunny conditions, the ocean surface can warm by a degree or more over the course of a few hours, with most of the stratification confined to the upper meter; this warm layer is stable, allowing evaporation to produce a much smaller (in density terms)

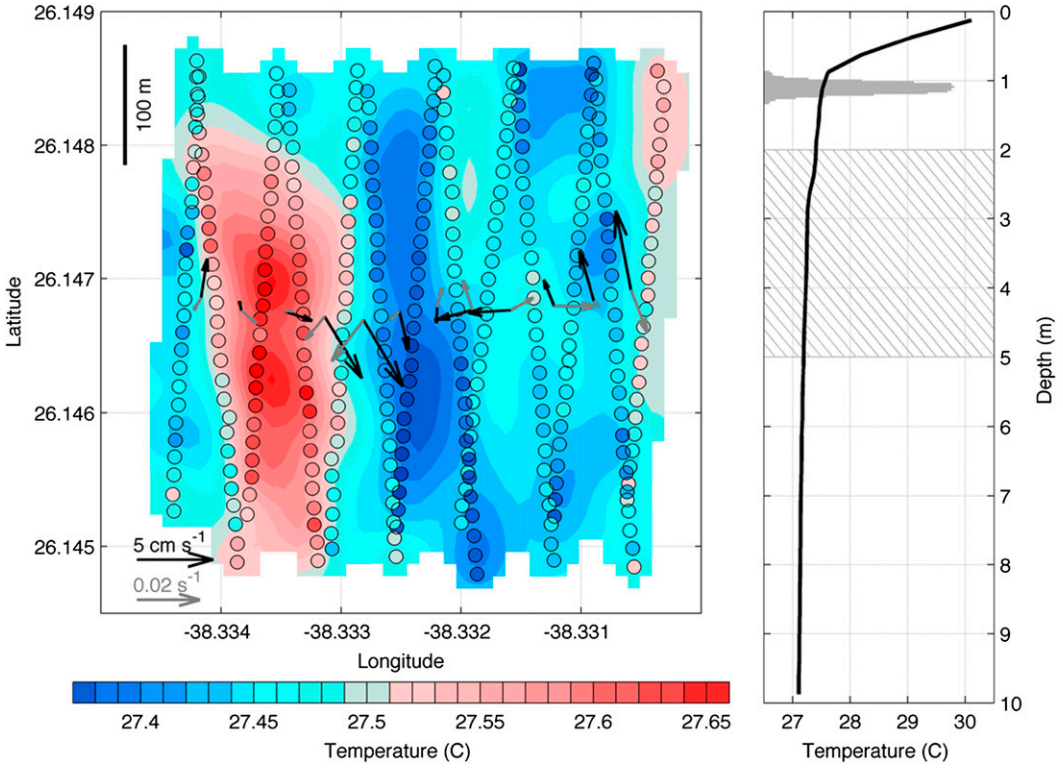

FIG. 4. (left) Objective map of temperature at 1.1 m below the surface. The vehicle deviated from this surface by 6 cm RMS, and the effect of these deviations is corrected for using the local vertical temperature gradient prior to mapping. Circles mark the locations of boxcar-averaged measurements (shown as fill color) used in the map, black arrows show the average current inferred from each north–south round trip, and gray arrows the vertical shear between 2- and 5-m depth, also averaged over consecutive northward and southward transects. Note the internal wave crest and trough. (right) Average temperature profile from the entire mission. The gray histogram represents the depths at which the measurements used in constructing the map were made. The cross-hatching denotes the layer over which the shear vectors shown at left were calculated. Note the extreme stratification in the upper meter.

increase in surface salinity. As the wind speed increases and/or the insolation decreases, the surface signature deepens and weakens, eventually disappearing under the influence of convection and mixing. These observations of the low-wind diurnal cycle largely confirm the conclusions of previous investigators (e.g., Soloviev and Lukas 1997); the dataset presented here may be unique, however, in its combination of duration and temporal resolution, its relative freedom from the contamination of artificially induced mixing, and its inclusion of salinity.

4. Internal waves on the diurnal pycnocline

Coherent, wavelike bands of higher and lower temperature have been observed in infrared observations of the surface of the ocean while a diurnal warm layer was present (e.g., Walsh et al. 1998). Farrar et al. (2007) linked such SST structures to internal waves on the diurnal pycnocline, but as they point out, the mechanism is more complex than simple advection of vertical temperature structure; according to classical internal wave theory, fluid particles on the surface remain on the surface. The SST bands are rather thought to be generated by a secondary process, such as the modulation of vertical mixing as the internal waves displace the base of the diurnal warm layer (Farrar et al. 2007). Beneath the surface, internal wave motion does directly produce temperature fluctuations on isobars; these subsurface temperature signatures may then be more straightforward to interpret than the surface bands. Here, we present AUV observations of wavelike temperature structures approximately 1 m below the ocean surface.

In an experiment designed to characterize the two-dimensional horizontal subsurface thermohaline structure within the diurnal warm layer, an EcoMapper was deployed at 1600 UTC 30 September 2012 on a lawnmower-type survey mission. The first leg of the mission, an undulation between the surface and 10-m depth, took the vehicle well into undisturbed water where it began a survey of a 450-m square at a nominal depth of 1 m (Fig. 4). The survey comprised 13 meridional transects 1.1 m below the surface, starting at the western

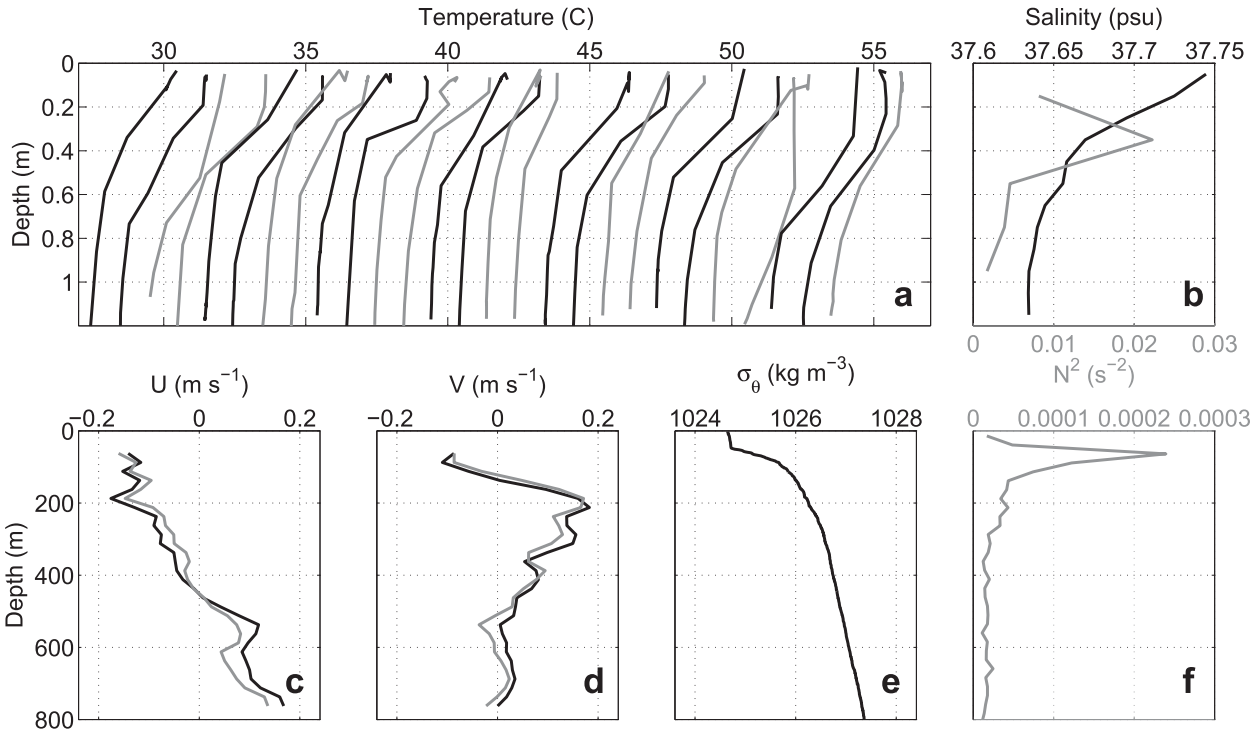

FIG. 5. (a) Temperature profiles, in chronological order, from each end of each transect of the 30 Sep 2012 AUV survey. Profiles are drawn through data points in the order they were sampled, rather than in order of decreasing pressure. Black profiles correspond to the northern ends of transects, and gray profiles correspond to the southern ends. Each successive profile is offset by 1°C. Transects were completed in order from west to east. The fourth-to-last profile is contaminated by ship-induced mixing. (b) The 10-cm binned mean of the salinity profiles (black) corresponding to the temperature records shown in (a); 20-cm binned mean square buoyancy frequency N^2 (gray) calculated from the mean temperature and salinity profiles. (c) The 25-m and 1-h binned mean zonal current speed profiles (positive eastward) from shipboard ADCP, corresponding approximately to the start (black) and end (gray) of the lawnmower survey. (d) Meridional current speed profiles (positive northward) plotted as in (c). (e) Potential density profile measured from the research vessel during the survey. (f) The N^2 profile computed from (e) and averaged in 15-m bins.

edge of the box and working eastward, which were connected by short turnaround segments at the surface, allowing for periodic GPS fixes and profiles of the upper meter. While submerged, the speed of the AUV was $1.7\,m\,s^{-1}$; at the surface it slowed to $1.3\,m\,s^{-1}$. The lawnmower pattern took approximately 80 min to complete.

The low-wind ($<2\,m\,s^{-1}$) conditions and clear skies during the survey and in the hours prior warmed the surface by an average of 3°C relative to the mixed layer below. Profiles to a depth of 10 m at the start of the survey and a concurrent shipboard CTD cast nearby established the bulk temperature of the upper mixed layer as approximately 27.1°C; surface temperatures as high as 30.8°C were recorded at some locations within the survey box. The corresponding increase in salinity was approximately 0.1 psu. Most of this stratification was confined to the upper meter (Figs. 5a,b), with a maximum vertical temperature gradient of $\sim 7°C\,m^{-1}$ at a depth of 40 cm, where the squared buoyancy frequency N^2 peaked near $0.02\,s^{-2}$ (Fig. 5b). The squared buoyancy frequency was smaller by more than an order of magnitude at the 1.1-m depth of the survey, averaging $10^{-3}\,s^{-2}$, but it was still much larger there than throughout the rest of the 46-m-deep mixed layer (Fig. 5e), where it was in the range of $10^{-5}\,s^{-2}$ (between a depth of 10 m and the base of the mixed layer, N^2 varied from 0.5×10^{-5} to $1.9 \times 10^{-5}\,s^{-2}$—see Fig. 5f). The AUV survey, then, was carried out within the diurnal warm layer—the temperature at 1.1 m averaged 0.4°C warmer than the bulk mixed layer—but below the depth of the most dramatic vertical gradients. The fourth-to-last profile in Fig. 5a appears to show less stratification near the surface and more at 1-m depth than the others; this is the result of mixing induced as the research vessel maneuvered near the southeast corner of the survey box in preparation for AUV recovery. Until the final two legs of the mission, the ship was positioned well to the northwest of the survey area where it could not contaminate the measurements.

Internal waves are the dominant features in the plan view of 1.1-m temperature measurements recorded

during the survey (Fig. 4) and were responsible, we believe, for bandlike surface slicks observed concurrently from the research vessel. The temperature distribution shown in the figure is an isotropic objective map, using a decorrelation length scale of 33 m, of all measurements made within 20 cm of a depth of 1.1 m. The vehicle deviated from the 1.1-m isobar by 6 cm RMS; the temperature error produced by these deviations was corrected using the local vertical temperature gradient prior to mapping. Circles mark the locations of boxcar-averaged measurements used to make the map. Black arrows show average current estimates, calculated as described in section 2. These vectors do not reflect the mean current across all transects, which was approximately 15 cm s^{-1} to the west-northwest; this has been subtracted. To eliminate any bias introduced by possible water speed errors associated with slight miscalibration of the DVL, each current estimate is formed as an average of the results from consecutive northward and southward underwater legs. The clear anticyclonic rotation of the current vectors moving from west to east is consistent with a westward-propagating progressive internal wave. Oddly, the amplitude of the current velocity oscillation along wave crests/troughs appears larger than that perpendicular to them, contrary to the prediction of internal wave theory; the major axis of the ellipses traced out by fluid particles in internal waves are expected to align with the propagation direction (Gill 1982). Whether the anomalous velocity is the result of a concurrent physical process or an artifact of the spatiotemporal sampling distribution has not been determined.

The downward-looking DVL provided vehicle-relative estimates of water velocity in 20 1-m bins. The signal-to-noise ratio of these measurements was quite low, particularly in the deeper bins, but with sufficient averaging, the correlation of consecutive independent vertical shear estimates suggests that a meaningful differential signal can be extracted from the upper few bins. We expect, on the basis of internal wave theory, the direction of the vertical shear at any point in the water column to be 90° to the right of the fluid velocity produced by the wave (Gill 1982). Differencing the DVL velocities from the first (shallowest) and fourth bins yields an estimate of vertical shear over a 3-m layer centered 2.5 m below the AUV (3.6 m below the surface); the gray arrows in Fig. 4 represent averages of this shear over each consecutive pair of transects, thus corresponding one to one with the current estimates described above. For vertical internal wavelengths large compared to 3 m, we might expect these shear estimates to approximate the vertical shear at the depth of the AUV, and indeed, though they are noisy, there is a tendency for the shear vectors in Fig. 4 (gray) to orient to the right of the residual velocity vectors after the removal of the mean current (black).

The horizontal phase speed of a progressive internal wave on the diurnal pycnocline may be estimated by approximating the upper ocean as a two-layer system, with a thin light layer overlying a much thicker heavy layer. In this idealized model, the wave speed c is given by

$$c = \sqrt{g'H},$$

where H is the thickness of the upper layer, and g' is the reduced gravity, which is defined as the gravitational acceleration g multiplied by the fractional change in density ρ between the two layers:

$$g' = g\frac{\Delta\rho}{\rho}.$$

Taking $H = 0.5$ m, and assuming the upper layer is 2°C warmer and 0.05 psu saltier than the lower, gives 6 cm s^{-1} as a rough speed estimate.

The internal wave snapshot in Fig. 4 is not synoptic; the effective average eastward speed over ground v of the AUV during the survey was 9 cm s^{-1} (the instantaneous speed of the vehicle was much higher, but it spent most of its time traveling north or south). As the wave moved westward, due both to propagation through the water ($c = -6$ cm s^{-1}, defining eastward to be positive) and to advection by the mean current ($u = -14$ cm s^{-1}), an apparent foreshortening effect was produced. The observed wavelength λ_o is related to the true wavelength λ_t of the westward-traveling wave as follows (ignoring the small meridional velocity components):

$$\lambda_o = \lambda_t\frac{v}{v - c - u}.$$

Thus, the observed wavelength of ~400 m indicates that the actual horizontal wavelength λ_t was in the range of ~1300 m. This, together with the estimated phase speed c, implies a wave period of ~6 h. It should be emphasized that these estimates are subject to several compounding sources of error, resulting in large uncertainties. The ability to track propagating features would eliminate much of this uncertainty; given the opportunity to repeat this experiment, we would sample the survey box multiple times, either with a single vehicle, or, preferably, by staggering the start times of multiple vehicles.

Having obtained estimates of frequency and horizontal wavenumber from a semi-infinite two-layer model,

we now consider the vertical propagation exhibited by internal waves in the real (continuously stratified) ocean. The internal wave dispersion relation provides a theoretical vertical wavenumber as a function of the buoyancy frequency. Though highly dependent on depth, the value of the buoyancy frequency at 4 m, $N^2 = 10^{-4}\,s^{-2}$, corresponds to a vertical wavelength of ~40 m, which helps justify ignoring the 2.5-m vertical offset between the velocity and shear estimates above (unfortunately, the DVL velocity measurements are too noisy and too shallow to provide a direct estimate of vertical wavelength). Deeper in the water column, between 200 and 500 m, the buoyancy frequency, established by a shipboard CTD cast carried out during the AUV survey, was $\sim 2 \times 10^{-5}\,s^{-2}$, corresponding to a vertical wavelength of ~80 m. As the research vessel remained in the survey area for only approximately 2 h, temporal fluctuations in current velocity at the internal wave period could not be resolved by the shipboard ADCP; however, the observations do show quasi-regular spatial fluctuations in the 200–500 depth range with a vertical scale of ~100 m, with some indication of upward propagation. Features recorded in the meridional current profile appear slightly shallower in a 1-h average profile centered at 1723 UTC, near the end of the survey (gray line in Fig. 5d), than they do an hour earlier (black line). It is possible, then, that the bands observed in the AUV survey were shallow manifestations of high-mode internal waves on the main thermocline.

5. Conclusions

1) Research vessels, simply by their presence, destroy the delicate thermohaline structure that develops in the upper meters of the ocean under low-wind, high-insolation conditions. In the case of a vessel holding station for an extended period, the effect can extend outward more than a ship length in multiple directions. Small, fast AUVs are effective at overcoming this difficulty. They facilitate uncontaminated observations, enabling both repeated profiles in a single location and resolution of two-dimensional small-scale subsurface horizontal structure.
2) The low-wind diurnal cycle of temperature and salinity in the upper few meters of the ocean was recorded over an 18-h period at subhour temporal resolution. Starting early in the day from a well-mixed state, the formation and eventual decay of a warm, salty upper layer was observed. Heat flux and evaporation implications of these observations were corroborated by measurements made at a nearby flux mooring.
3) A subsurface, two-dimensional small-scale horizontal map of the diurnal pycnocline has been captured. It shows both the temperature signature of displaced isopycnals and the velocity and shear characteristics of progressive internal waves. The estimated vertical wavenumber of these waves is roughly consistent with vertical fluctuations in concurrent shipboard ADCP observations, suggesting that, rather than wind-driven variability confined to the diurnal warm layer, the waves may extend into the thermocline.

Given the importance of diurnal warm layer dynamics to air–sea fluxes and the interpretation of remote sensing datasets and the ongoing development of relatively low-cost AUVs and associated sensors, we foresee an expanding role for AUVs in diurnal warm layer sampling. While the single lawnmower-type survey of the diurnal warm layer yielded interesting results, interpretation would be facilitated by multiple occupations of the survey box, which would allow propagating features to be tracked. Future work will focus on resolving a truly four-dimensional picture of the layer, showing the evolution in time of both horizontal features and vertical structure.

Acknowledgments. NASA supported this work under Grant NNX11AE82G. We thank the captain and crew of the R/V *Knorr* for their able assistance in this endeavor. Tom Farrar provided useful comments, and we are grateful for the help of two anonymous reviewers.

REFERENCES

Farrar, J. T., C. J. Zappa, R. A. Weller, and A. T. Jessup, 2007: Sea surface temperature signatures of oceanic internal waves in low winds. *J. Geophys. Res.,* **112,** C06014, doi:10.1029/2006JC003947.

Gill, A. E., 1982: *Atmosphere–Ocean Dynamics*. Academic Press, 662 pp.

Halpern, D., and R. K. Reed, 1976: Heat budget of the upper ocean under light winds. *J. Phys. Oceanogr.,* **6,** 972–975, doi:10.1175/1520-0485(1976)006<0972:HBOTUO>2.0.CO;2.

Jacobs, W. C., 1942: On the energy exchange between sea and atmosphere. *J. Mar. Res.,* **5,** 37–66.

Morison, J., R. Andersen, N. Larson, E. D'Asaro, and T. Boyd, 1994: The correction for thermal-lag effects in Sea-Bird CTD data. *J. Atmos. Oceanic Technol.,* **11,** 1151–1164, doi:10.1175/1520-0426(1994)011<1151:TCFTLE>2.0.CO;2.

Price, J. F., R. A. Weller, and R. Pinkel, 1986: Diurnal cycling: Observations and models of the upper ocean response to diurnal heating, cooling, and wind mixing. *J. Geophys. Res.,* **91,** 8411–8427, doi:10.1029/JC091iC07p08411.

Soloviev, A., and R. Lukas, 1997: Observation of large diurnal warming events in the near-surface layer of the western equatorial Pacific warm pool. *Deep-Sea Res. I,* **44,** 1055–1076, doi:10.1016/S0967-0637(96)00124-0.

Stramma, L., P. Cornillon, R. A. Weller, J. F. Price, and M. G. Briscoe, 1986: Large diurnal sea surface temperature

variability: Satellite and in situ measurements. *J. Phys. Oceanogr.,* **16,** 827–837, doi:10.1175/1520-0485(1986)016<0827:LDSSTV>2.0.CO;2.

Stuart-Menteth, A. C., I. S. Robinson, and P. G. Challenor, 2003: A global study of diurnal warming using satellite-derived sea surface temperature. *J. Geophys. Res.,* **108,** 3155, doi:10.1029/2002JC001534.

Walsh, E. J., R. Pinkel, D. E. Hagan, R. A. Weller, C. W. Fairall, D. P. Rogers, S. P. Burns, and M. Baumgartner, 1998: Coupling of internal waves on the main thermocline to the diurnal surface layer and sea surface temperature during the tropical ocean—Global atmosphere coupled ocean–atmosphere response experiment. *J. Geophys. Res.,* **103,** 12 613–12 628, doi:10.1029/98JC00894.

Webster, P. J., C. A. Clayson, and J. A. Curry, 1996: Clouds, radiation, and the diurnal cycle of sea surface temperature in the tropical western Pacific. *J. Climate,* **9,** 1712–1730, doi:10.1175/1520-0442(1996)009<1712:CRATDC>2.0.CO;2.